JOURNAL OF NANO- AND ELECTRONIC PHYSICS
Vol. **4** No 4, 04028(5pp) (2012)

ЖУРНАЛ НАНО- ТА ЕЛЕКТРОННОЇ ФІЗИКИ
Том **4** № 4, 04028(5cc) (2012)

Effect of Mg Doping on the Structural and Optical Properties of CdS Nanoparticles Synthesized by co-Precipitation Method

G. Giribabu[1], G. Murali[1], D. Amaranatha Reddy[1], R.P. Vijayalakshmi[1,*], N. Madhusudhana Rao[2,†]

[1] *Dept. of Physics, Sri Venkateswara University, Tirupati, 517502 India*
[2] *School of Advanced Sciences, VIT University, Vellore, 632014 India*

(Received 11 November 2012; published online 29 December 2012)

$Cd_{1-x}Mg_xS$ ($x = 0.00$, 0.05, 0.10, 0.15 and 0.20) nanoparticles were synthesized by co-precipitation method for the first time. Compositional, morphological, structural and optical studies of the as prepared samples were carried out by X-ray diffraction (XRD), Energy dispersive analysis of X-rays (EDAX), Scanning electron microscopy (SEM), Diffuse reflectance spectroscopy (DRS) and Photoluminescence (PL) techniques. XRD studies revealed the structural phase transition from cubic to hexagonal and increase in the average grain size of the nanoparticles (lie in the range 1.4 nm to 2.8 nm) with increasing Mg content. EDAX spectra rules out the existence of impurities in the samples. Bandgap widening was observed in all the samples compared to bulk CdS (2.42 eV). Decrease in bandgap (3.02 eV to 2.54 eV), luminescence quenching and red shift of luminescence peak position were observed with increasing Mg in $Cd_{1-x}Mg_xS$.

Keywords: Mg doped CdS, Co-precipitation, Phase transition, Bandgap.

PACS numbers: 64.70.Nd, 81.07.Bc

1. INTRODUCTION

Sulphur based binary chalcogenide semiconductors like ZnS and CdS have attracted much attention in the past few decades due to their unique properties. In semiconductor nanoparticles if the particle size is greater than Bohr exciton radius it is said to be in weak confinement regime. If the particle size is reduced below the Bohr exciton radius it is said to be in strong confinement regime. Quantum confinement leads to new electronic states in the band structure of semiconductor. Semiconductor nanoparticles exhibit different electrical and optical properties from those of their bulk due to quantum confinement [1]. CdS is one among the II-VI semiconductors with wide bandgap (2.42 eV) [2] at room temperature and Bohr exciton radius ≈ 3 nm. CdS has been extensively studied in the past few decades due to its applications in various fields like X-ray detectors, window material for hetero junction solar cells, light emitting diodes, photocatalysis, biological sensors, address decoders and gas detectors [3-9]. CdS has hexagonal wurtzite crystal structure in bulk form where as other two structures (cubic zincblende and rocksalt) are observed only in nanocrystalline form [10].

Mg doped ZnO nanocrystals were synthesized by several methods like chemical co-precipitation, sol-gel, direct thermal deposition, sono chemical and femto second laser ablation [11-15]. Vinodkumar et al. fabricated Mg doped ZnO nanoparticles for efficient sunlight driven photocatalysis [16]. Many workers reported bandgap widening and blue shift of the PL emission peak in Mg doped ZnO nanoparticles [17-20]. But decrease in bandgap and corresponding red shift of the PL emission peak was reported by Junlin Li et al. in Mg doped ZnO micro prisms [21] and by R.Viswanathan et al. in Mg doped ZnO nanoparticles [22]. Synthesis of Mg doped ZnS quantum dots was reported by Zhong et al. by precipitation method [23].Temperature dependent photoluminescence of Mg doped CdS nanowires was reported by Jun Zhang et al. [24]. No reports are available about the synthesis of Mg doped CdS nanoparticles. We synthesized Mg doped CdS nanoparticles via chemical co precipitation method for the first time.

2. EXPERIMENTAL

All the chemicals used in the synthesis of present nanoparticles were of analytical grade (AR) and were used without further purification. Sodium sulfide (Na_2S), cadmium acetate di hydrate ($Cd(CH_3COO)_2.2H_2O$) and magnesium acetate tetra hydrate ($Mg(CH_3COO)_2.4H_2O$) were used as precursors. Double distilled de ionized water was used as solvent and 2 mercaptoethanol ($HOCH_2CH_2SH$) was used as surfactant.

$Cd_{1-x}Mg_xS$ ($x = 0.00$, 0.05, 0.10, 0.15 and 0.20) nanoparticles were prepared by taking 50 ml aqueous solution of acetates (Cd and Mg) as per the stoichiometric ratio (0.2 M) and 1 ml capping agent is added to it.50 ml of aqueous sodium sulfide solution (0.2 M) was added drop wise to the above solution at 80 °C temperature under constant stirring for 2 hours. Filtered precipitates were dried in vacuum for 8 hours at 60 °C and made in to fine powders.

Crystal structure of the synthesized nano particles was studied using Serifert 3003 TT X-ray Diffractometer with Cu-Kα radiation with a wavelength of 1.540 Å. Chemical composition and surface morphology of the target samples were analysed using Scanning Electron Microscope (SEM) with Energy Dispersive Analysis of X-rays (EDS) attachment (CARL-ZESIS EVO MA 15). Diffuse reflectance measurements of dry powders were performed using Jasco V-670 double-beam spectrophotometer for energy gap determination. Photo-luminescence (PL) studies were carried out using JOBIN-YVON Fluorolog-3 Spectrophotometer with a 450 W Xenon arc lamp as an excitation source.

* vijayaraguru@gmail.com
† drnmrao@gmail.com

3. RESULTS AND DISCUSSION

3.1 Elemental Analysis

Fig. 1a and b shows the EDAX spectra of $Cd_{1-x}Mg_xS$ ($x = 0.00$ and $x = 0.10$) nanoparticles. In the synthesized samples elemental Cd, S and Mg were found in a near stoichiometric ratio. No traces of other elements were noticed in the spectra confirming the purity of the samples.

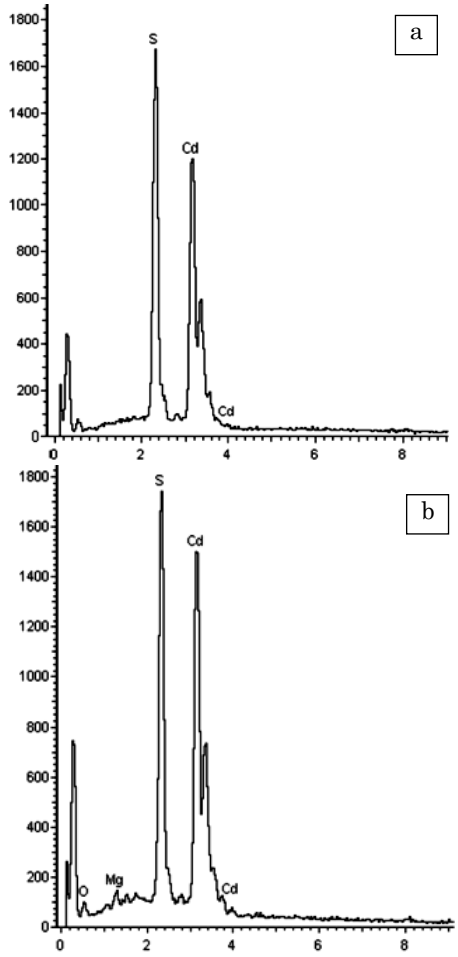

Fig. 1 – EDAX Spectra of (a) Pure CdS and (b) $Cd_{0.90}$ $Mg_{0.10}S$ nanoparticles

3.2 Morphological Analysis

SEM is a powerful tool to study the surface morphology of the samples. Fig. 2a and 2b represents the SEM images of pure CdS and $Cd_{0.80}Mg_{0.20}S$ nanoparticles. From the images it is evident that in un-doped sample only clusters of agglomerated particles are seen, where as in Mg doped sample agglomeration was decreased with uniform distribution of particles.

3.3 Structural Analysis

Fig. 3a shows the x-ray diffraction patterns of the prepared samples. For pure CdS and $Cd_{0.95}Mg_{0.05}S$ nanoparticles, the x-ray diffraction pattern consists of two broad peaks centred at 2θ values 27° and 47°. They can be indexed to the cubic zincblende structure. Similar structure was reported by Herron et al. [25] and

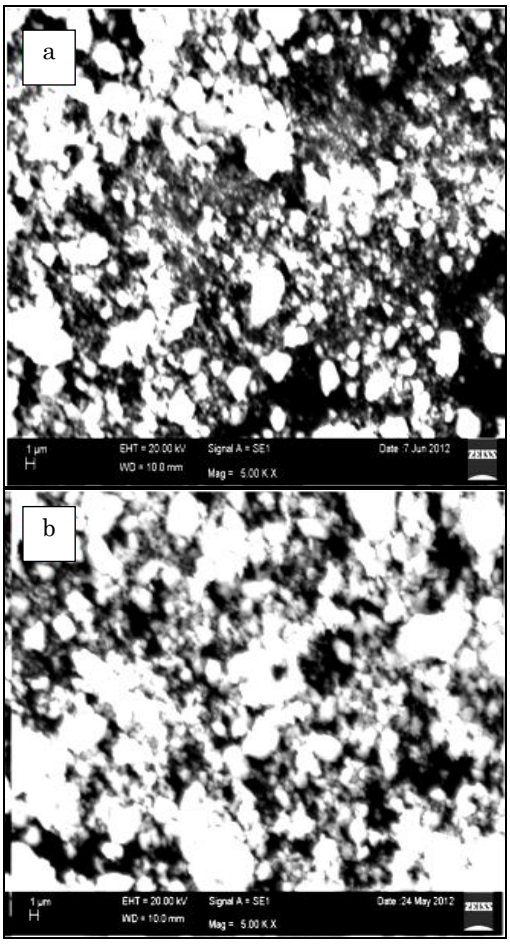

Fig. 2 – SEM images of (a) Pure CdS and (b) $Cd_{0.80}Mg_{0.20}S$ nanoparticles

Banerjee et al. [26] in pure CdS nanoparticles. X-ray diffraction pattern of $Cd_{0.90}Mg_{0.10}S$ consists of multiple peaks with overlapping. So we are not able to index them either to cubic or to hexagonal phase. This pattern may be due to the mixture of both cubic and hexagonal phases. Three distinct peaks were observed in $Cd_{0.85}Mg_{0.15}S$ and $Cd_{0.80}Mg_{0.20}S$ at 2θ values 26.6°, 43.6° and 51.8° can be indexed to the (002), (110) and (112) planes of hexagonal phase (JCPDS CARD.NO.02-0549). Thus by doping Mg in to CdS, structure is transformed from cubic to hexagonal phase and the transition is observed at $x = 0.01$. The cubic and hexagonal structures are polytypic. Structural transformation occurs easily by introducing stacking faults. The stacking fault energy (SFE) of CdS is in the range of 8.7 mJm^{-2} [27]. In our samples stacking fault energy seems to be still decreasing and particles precipitate at higher rates. So the stacking faults may be easily introduced while synthesizing Mg doped CdS nanoparticles which lead to structural transition from cubic to hexagonal. We noticed that diffraction peaks shifted towards higher 2θ values with increasing Mg content. This may be due to the smaller ionic radii of Mg^{2+} (0.57 Å) when compared to Cd^{2+} (0.96 Å). This shift confirms that the doped Mg substitutes Cd in Mg doped CdS samples. The average grain size of the nanoparticles was calculated using Scherrer formula [28].

$$D = 0.89\lambda / \beta \cos\theta$$

where D is the average particle size, λ is wavelength of Cu-Kα irradiation, β is the full width at half maximum intensity of the diffraction peak and θ is the diffraction angle. The calculated diameters of the particles ranging from 1.4 nm to 2.8 nm were listed in Table 1. From the table it is evident that the particle size (D) increases with increasing x in $Cd_{1-x}Mg_xS$. Variation of particle size D with Mg content x in the samples is shown in Fig. 3b.

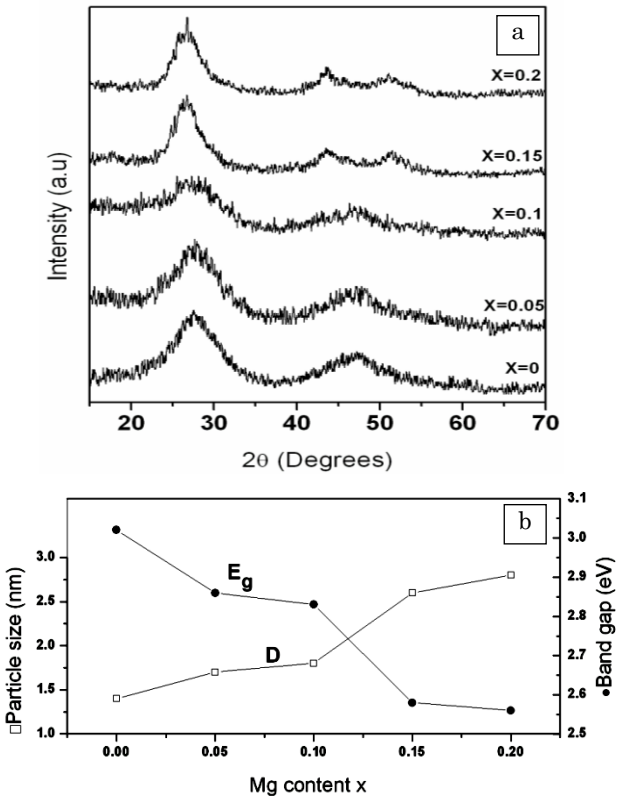

Fig. 3 – XRD spectra of $Cd_{1-x}Mg_xS$ ($x = 0.00$, 0.05, 0.10, 0.15 and 0.20) nanoparticles (a). Variation of particle size D and band gap Eg with Mg content x (b)

Table 1 – Partcle size (D), bandgap (E_g) and wavelength of PL peak (λ) of $Cd_{1-x}Mg_xS$ ($x = 0.00$, 0.05, 0.10, 0.15 and 0.20) nanoparticles

Mg Composition x	Particle Size D (nm)	Bandgap E_g (eV)	λ for PL peak (nm)
0.00	1.4	3.02	405
0.05	1.7	2.86	514
0.10	1.8	2.83	523
0.15	2.6	2.58	545
0.20	2.8	2.56	548

In the present study we observed cubic phase in finer particles and hexagonal phase in coarser particles (Mg doped). Banerjee et al. reported size induced structural transition in CdS nanoparticles [26]. The structural transition observed here in our samples can also be associated with the variation of particle size with Mg doping.

3.4 DRS Analysis

Fig. 4a shows the room temperature diffuse reflectance spectra for the as synthesized nanoparticles. The absorption edges are seen to be shifted towards higher wavelengths/lower energies with increasing Mg content. Two absorption edges present in the DRS spectra for the sample $Cd_{1-x}Mg_xS$ ($x = 0.10$) confirms the coexistence of cubical and hexagonal phases supported by the XRD analysis.

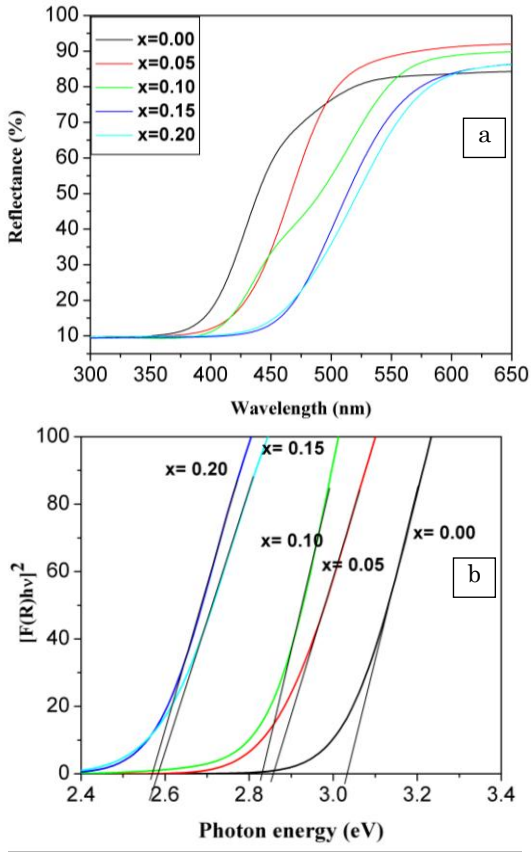

Fig. 4 – Diffuse Reflectance Spectra of $Cd_{1-x}Mg_xS$ ($x = 0.00$, 0.05, 0.10, 0.15 and 0.20) nanoparticles (a). Kubelka-Munk plots for bandgap estimation of $Cd_{1-x}Mg_xS$ ($x = 0.00$, 0.05, 0.10, 0.15 and 0.20) nanoparticles (b)

For analysis purposes the diffuse-reflectance (R) of the sample can be related to the Kubelka–Munk function $F(R)$ by the relation $F(R) = (1 - R)^2 / 2R$ [29]. The bandgap of the pure and Mg doped nanoparticles was estimated from the diffuse-reflectance spectra by plotting the square of the Kubelka-Munk function $F(R)^2$ versus energy and extrapolating the linear part of the curve to $F(R)^2 = 0$, as shown in Fig. 4b. The bandgap values estimated for the $Cd_{1-x}Mg_xS$ ($x = 0.00$, 0.05, 0.10, 0.15 and 0.20) nanoparticles are in the range 3.02 to 2.56 eV and were mentioned in Table 1. These values are higher than that of bulk CdS (2.42 eV) which can be attributed to the quantum confinement effect. Bandgap widening also confirms the nano form of the target samples. It is clear from the Fig. 4b that bandgap is decreasing with the increasing Mg content in CdS. Variation of bandgap may be due to the increase of particle size with increasing Mg content. Variation of bandgap with Mg content x is shown in Fig. 3b.

3.5 Photoluminescence Analysis

Photoluminescence emission spectrum for pure CdS nanoparticles is shown in Fig. 5a. Visible violet luminescence was observed with emission peak at 405 nm. This can be attributed to the band edge emission. As the material is excited with certain wavelength, the absorption of photons creates electron and hole pairs. The band edge emission is due to the recombination of electron and hole pairs in the nanoparticles. Tian et al. were also reported violet band edge emission in CdS nanoparticles of size 2.6 nm [30]. Another small hump is also observed at wavelength of 480 nm may be due to the interstitial defects. Fig. 5b represents the PL excitation spectrum of pure CdS with peak at 353 nm.

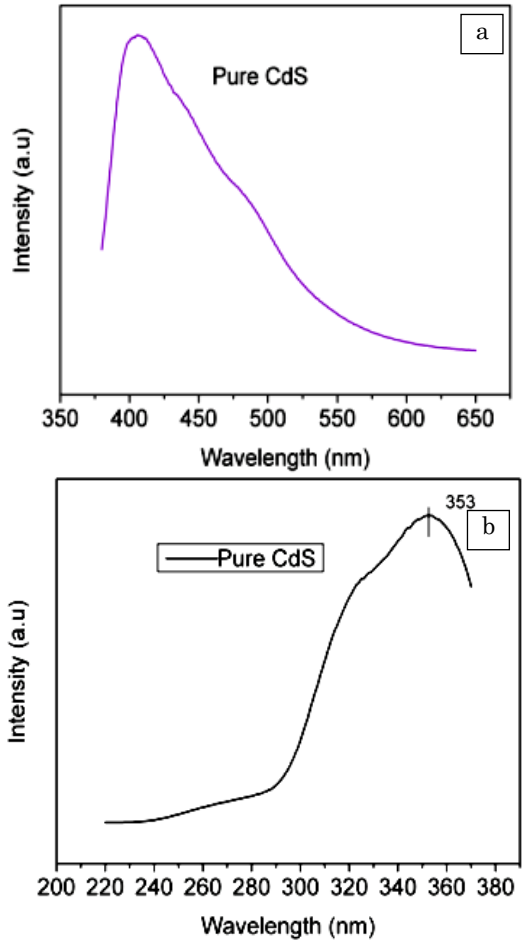

Fig. 5 – PL Emission Spectrum (a) and PL Excitation Spectrum of Pure CdS nanoparticles (b)

PL emission spectra of Mg doped CdS nanoparticles are shown in Fig. 6a. No band edge emission was observed in Mg doped samples. All the Mg doped samples exhibited strong green emission with luminescence quenching and very weak red emission. Green emission can be associated with defects in the crystallization process due to the incorporation of Mg or / and interstitial sulphur [24, 31]. Luminescence quenching with increasing Mg content may be due to the formation of deep level traps. Peak position of the green emission is red shifted from 512 nm to 548 nm with increasing Mg content. Details of this red shift is listed in Table 1. This red shift can be associated with the decrease in bandgap. There were no reports on Mg doped CdS nanoparticles for comparison. Similar type of decreasing bang gap and red shift of PL emission peak was reported in ZnO micro prisms doped with Mg [21], ZnO nanoparticles doped with Mg [22] and CdS nanoparticles doped with Cr [32]. Red emission in the range 650-680 nm can be attributed to trapped luminescence or surface states [24]. Fig. 6b shows the excitation spectra of $Cd_{1-x}Mg_xS$ ($x = 0.05$ and 0.20). From the figure it is observed that the excitation peak is shifted from 393 to 421 nm with increasing Mg content. PL excitation spectra (PLE) measured reveals a linear increase in the peak wavelength with increasing Mg doping levels. The dependence of the optical band gap on Mg concentration derived from reflectance spectra and the PLE spectra correspond well with each other.

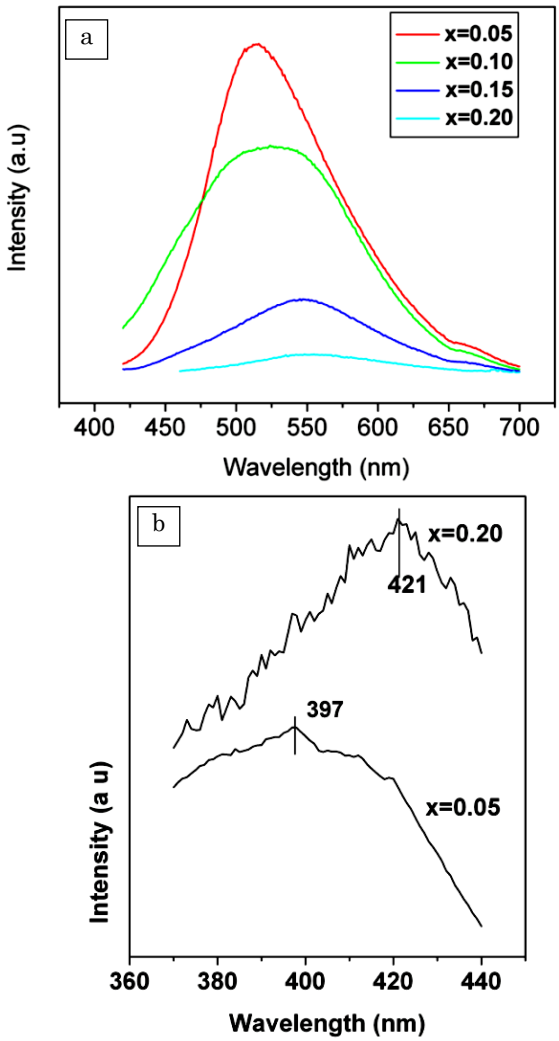

Fig. 6 – PL Emission Spectra of $Cd_{1-x}Mg_xS$ ($x = 0.00$, 0.05, 0.10, 0.15 0.20) (a). PL Excitation Spectra of $Cd_{1-x}Mg_xS$ ($x = 0.05$, and 0.20) nanoparticles

4. CONCLUSION

Intrinsic and Mg doped CdS nanoparticles were successfully synthesized by simple co-precipitation method. Dopant induced structural transformation from cubic to hexagonal phase was revealed by the X-ray diffraction pattern. All the samples exhibited

bandgap widening when compared to bulk CdS (2.42 eV). Mg doped CdS nanoparticles evidenced strong green emission and very weak red emission. Decrease in bandgap, increase in particle size, luminescence quenching and red shift of PL peak position was observed with increasing Mg content in CdS.

AKNOWLEDGEMENTS

G. Giribabu is grateful for support from the University Grant Commission New Delhi India for awarding Teacher Fellowship under Faculty Development Programme.

REFERENCES

1. U. Woggon, *Optical Properties of Semiconductor Quantum Dots* p. 136 (Berlin: Springer-Verlag Publishing: 1997).
2. A. Phuruangrat, T. Thongtem, S. Thongtem, *Mater. Lett.* **63**, 1538 (2009).
3. R. Frerichs, *J. Appl. Phys.* **21**, 312 (1950).
4. I.O. Oladeji, L. Chow, C. Ferekides, V. Viswanathan, Z. Zhao, *Sol. Energ. Mat. Sol. C.* **61**, 203 (2000).
5. H. Murai, T. Abe, J. Matsuda, H. Sato, S. Chiba, Y. Kashiwaba, *Appl. Surf. Sci.* **244**, 351 (2005).
6. Z. Zhang, *J. Colloid Interf. Sci.* **356**, 783 (2011).
7. M. BruchezJr, M. Moronne, P. Gin, S. Weiss, A.P. Alivisatos, *Science* **281**, 2013 (1998).
8. Z.H. Zhong, D.L. Wang, Y. Cui, M.W. Bockrath, M.C. Lieber, *Science* **302**, 1377 (2003).
9. H.H. Afify, I.K. Battisha, *J. Mater. Sci- Mater. El.* **11**, 373 (2000).
10. P. Villars, L.D. Calvert (eds) *Pearson's Handbook of Crystallographic Data for Intermetallic Phases vol 2.* (Metals Park, OH: ASM International: 1985).
11. N. Kilinc, L. Arda, S. Ozturk, Z.Z. Oztürk, *Cryst. Res. Technol.* **45**, 529 (2010).
12. B. Karthikeyan, T. Pandiyarajan, *J. Lumin.* **130**, 2317 (2010).
13. S. Labuayai, V. Promark, S. Maensiria, *Optoelectron. Adv. Mater. Rapid Commun.* **2**, 798 (2008).
14. Huan-Ming Xiong, Dmitry G. Shchukin, Helmuth Möhwald, Yang Xu, Yong-Yao Xia, *Angew. Chem. Int. Edit.* **48**, 2727 (2009).
15. E. Chelnokov, M. Rivoal, Y. Colignon, D. Gachet, L. Bekere, F. Thibaudau, S. Giorgio, V. Khodorkovsky, W. Marine, *Appl. Surf. Sci.* **258**, 9408 (2012).
16. Vinodkumar Etacheri, Roshith Roshan, Vishwanathan Kumar, *ACS Appl. Mater. Interf.* **4**, 2717 (2012).
17. W.Q. Peng, S.C. Qu, G.W. Cong, Z.G. Wang, *Appl. Phys. Lett.* **88**, 101902 (2006).
18. Talaat M. Hammad, Jamil K. Salem, *J. Nanopart. Res.* **13**, 2205 (2011).
19. Y.S. Wang, P. John Thomas, P. O'Brien, *J. Phys. Chem. B.* **110**, 21412 (2006).
20. Hui Li, Yongzhe Zhang, Xiaojun Pan, Hongliang Zhang Tao Wang, Erqing Xie, *J. Nanopart. Res.* **11**, 917 (2009).
21. Junlin Li, Huizhao Zhuang, Jie Wang, Peng Xu, *Appl. Surf. Sci.* **257**, 2337 (2011).
22. R. Viswanatha, Y. Arthoba Nayaka, C.C. Vidyasagar, T.G. Venkatesh, *J. Chem. Pharm. Res.* **4**, 1983 (2012).
23. Zhong Chen, Xiao Xia Li, Nan Chen, Guoping Du, Yangsheng Li, Guihua Liu, Andy Y.M. Suen, *J. Mat. Sci. Eng. B-Adv.* **177**, 337 (2012).
24. Jun Zhang, Feihong Jiang, *Phys. Lett. A.* **373**, 3888 (2009).
25. N. Herron, Y. Wang, H. Eckert, *J. Am. Chem. Soc.* **112**, 1322 (1990).
26. R. Banerjee, R. Jayakrishnan, P. Ayyub, *J. Phys.: Condens. Matter* **12**, 10647 (2000).
27. S. Takeuchi, K. Suzuki, *phys. status solidi a* **171**, 99 (1999).
28. B.D. Cullity, *Elements of X-ray Diffraction, Second ed.*, (New York: Addison–Wesley Publishing: Reading, MA: 1956).
29. A. Escobedo Morales, E. Sanchez Mora, U. Pal, *Rev. Mex. de Fisica* **S53**, 18 (2007).
30. I. Luisetto, F. Pepe, E. Bemporad, *J. Nanopart. Res.* **10**, 59 (2008).
31. Vineet Singh, Pratima Chauhan, *J. Phys. Chem. Solids* **70**, 1074 (2009).
32. Punita Srivastava, Pushpendra Kumar, Kedar Singh, *J. Nanopart. Res.* **13**, 5077 (2011).